Taylor & Francis
Taylor & Francis Group

Mining Technology

Transactions of the Institutions of Mining and Metallurgy

ISSN: (Print) (Online) Journal homepage: https://www.tandfonline.com/loi/ymnt21

Measuring blast fragmentation at Nui Phao open-pit mine, Vietnam using the Mask R-CNN deep learning model

Trong Vu, Tran Bao, Quoc Viet Hoang, Carsten Drebenstetd, Pham Van Hoa & Hoang Hung Thang

To cite this article: Trong Vu, Tran Bao, Quoc Viet Hoang, Carsten Drebenstetd, Pham Van Hoa & Hoang Hung Thang (2021): Measuring blast fragmentation at Nui Phao open-pit mine, Vietnam using the Mask R-CNN deep learning model, Mining Technology, DOI: 10.1080/25726668.2021.1944458

To link to this article: https://doi.org/10.1080/25726668.2021.1944458

MINING TECHNOLOGY
https://doi.org/10.1080/25726668.2021.1944458

Measuring blast fragmentation at Nui Phao open-pit mine, Vietnam using the Mask R-CNN deep learning model

Trong Vu [a], Tran Bao[b], Quoc Viet Hoang[c], Carsten Drebenstedt[d], Pham Van Hoa[b] and Hoang Hung Thang[a]

[a]Surface Mining Department, Quang Ninh University of Industry, Dong Trieu, Vietnam; [b]Surface Mining Department, Hanoi University of Mining and Geology, Hanoi, Vietnam; [c]School of Resources and Safety Engineering, Central South University-Hunan Changsha, Changsha, People's Republic of China; [d]Surface Mining Department, TU Bergakademie Freiberg, Freiberg, Germany

ABSTRACT

Blast fragmentation size distribution is one of the most critical factors in evaluating the blasting results and affecting the downstream mining and processing operations in open-pit mines. Image-based methods are widely applied to address the problem but require heavy user interaction and experience. This study deployed a deep learning model Mask R-CNN to develop an automatic measurement method of blast fragmentation. The model was trained using images captured from real blasting sites in Nui Phao open-pit mine in Vietnam. The trained model reported high average precision scores (Intersection over Union, IoU = 0.5) 92% and 83% for bounding box and segmentation masks, respectively. The results lay a solid technical basis for the automated measurement of blast fragmentation in open-pit mines.

ARTICLE HISTORY
Received 7 April 2021
Revised 8 June 2021
Accepted 9 June 2021

KEYWORDS
Blast fragmentation measurement; open-pit mine; deep learning; image-based method; Mask R-CNN

Introduction

Rock blast fragmentation measurement is the central task to evaluate blasting results in the mining industry. This measurement supplies valuable information for optimising blasting and downstream operations, including digging, loading, hauling, and crushing. For process integration and optimisation methods, measurement of the run of mine fragmentation is essential for model calibration purposes and subsequent application in scenario-based simulations (Onederra et al. 2010). Typically, the measurement deploys cumulative passing size distribution (CDF) or sieving curve to represent muck pile fragmentation characteristics after blasting. The CDF curve describes the sieving analysis using screens with a known mesh size. The screen retains fragments larger than that mesh size and conversely. The fragments caught on each screen are then weighed and used to construct the CDF.

Blasting in mining usually generates a widespread muck pile containing thousands of fragments of various sizes and shapes. Whereas quick and accurate measurement is essential to analyse blasting fragmentation. Direct methods, such as sieving or screening, can give high accurate CDF of blasting fragmentation but is costly, time-consuming, and inconvenient (Sudhakar et al. 2006). Prediction methods have been applied widely. Some experimental fragmentation models, such as Larrson's equation, SveDeFo formula, or Kuzram model, are indirect methods that evaluate the blasting fragmentation, but their accuracy is questioned (Thornton et al., 2001; Chakraborty et al. 2004; Siddiqui 2009). Artificial Intelligence has gradually been utilised to predict blast fragmentation size in the past few years. Many researchers have been applied machine learning algorithms such as Support Vector Machine (Shi et al. 2012), fuzzy logic (Monjezi et al. 2009), Artificial Neural Network (Kulatilake et al. 2010; Sayadi et al. 2013; Enayatollahi et al. 2014) to develop their predictive fragmentation models. Nevertheless, the practicality of these models is a problem due to the complicated nature of blast parameters influencing fragmentation, such as blast design parameters, explosive properties, or rock mass properties.

In recent years, computer vision methods based on image processing have developed and become familiar. They implement the tasks referred to as instance segmentation, which localises and segments the rock fragments on digital images. Split Desktop, WipFrag, FragScan, and GoldSize are the most popular computer programs operating on these methods (Hunter et al. 1990). Computer vision methods are economically feasible and practical than direct methods. However, they cannot resolve fragments ranging in size from metres down to some microns. Consequently, they merge smaller fragments into larger ones or separate larger ones into smaller ones and result in a steeper or more uniform CDF than sieving (Hunter et al. 1990; Ouchterlony and Sanchidrián 2019; Schenk et al. 2019). Although some programmes introduce correction techniques to increase the quality of measurement, their results still strongly depend on user

CONTACT Trong Vu trongvu@qui.edu.vn Surface Mining Department, Quang Ninh University of Industry, Yen Tho, Dong Trieu, Quang Ninh, Vietnam

intervention, expert knowledge, and the form of image acquisition (Thornton et al., 2001; Chakraborty et al. 2004). Onederra et al. (2015) introduced 3D high-resolution laser scanning as an alternative technique to measure blast fragmentation and to improve 2D imaging systems. However, this method needs a high initial investment in hardware and training workers to operate the scanner and software.

In the past decade, computer vision has evolved dramatically using machine learning methods. The primary idea is to use deep learning frameworks trained using a massive volume of image data collected through sensors or the internet to understand precisely which real-word object makes up an image. Deep learning models like Fast/Faster R-CNN (Girshick 2015; Ren et al. 2015) and Fully Convolutional Network (FCN) (Long et al. 2015) are the core systems for segmentation and localisation of objects in the image, respectively. For example, DeepMask (Pinheiro et al. 2015), SharpMask (Pinheiro et al. 2016), and the following work (Dai et al. 2016) use Region-Based Convolutional Neural Networks (R-CNN) to segment objects and then Fast-RCNN to classify them. Dai et al. (2016) also proposed three hierarchical stages, including bounding-box proposals, segmentation, and classification. The problem with all these methods is slow and less accurate because of the distinct or sequential implementation of these detection steps.

Recently, Li et al. (2017) merged segment proposals and object detection in a system named 'fully convolutional instance segmentation' (FCIS) to fully convolutionally predict a set of position-sensitive output channels. Solving object class, boxes, and masks in one step make the system fast. Nevertheless, FCIS exposes the problem with overlapping instances and pseudo edges.

The deep learning model Mask R-CNN (He et al. 2017) is considered a state-of-art algorithm and outperforms others in the instance segmentation problem. It has shown that superior performance in natural object detection, but studies using Mask R-CNN in blasting fragmentation analysis is minimal. This application was first used by Fabian Schenk et al. (2019) to analyse the distribution of rock fragments in the blasting muck pile. The input image dataset was collected and trained in the laboratory before being tested on real-world large UAV images. The experiments were promising, but the accuracy in detecting small fragments need to be improved.

Our study explores the deep learning model Mask R-CNN to automatically and quickly measure blast fragmentation at a low cost. We trained the Mask R-CNN model only using annotation from digital images collected directly on mine sites and then conducted an inference to generate the final segmentation image. The trained Mask R-CNN was evaluated using two standard metrics in object detection to highlight the performance. Furthermore, the method is compared with the SplitDesktop software to assess the accuracy.

The paper proceeds as follows. Section 'Nui Phao open-pit mine, Vietnam' describes the study area, where Section 'Methodology' proposes the used method for blast fragmentation measurement. Section 'Results' presents the results. Discussion in section 'Discussion' and conclusion in section 'Conclusions' complete the paper.

Nui Phao open-pit mine, Vietnam

Nui Phao mine is located in the northern part of Vietnam in Thai Nguyen province, approximately 80 km northwest of Hanoi capital by road. The mine represents one of the world's largest identified tungsten reserve outside China. Nui Phao is a typical open-pit mine extracting 6.5 million m^3 materials with about 3.7 million ore in 2017. Of this, 3.5 m^3 required blasting. Figure 1 presents the location of the mine and the overview of its mining site.

The mine applies the bench blasting technique for breaking waste rock and ore. To measure the blast

Figure 1. Location and mining site of Nui Phao open-pit mine. 'Images are available in colour online.'

Figure 2. An example of image capture for blast fragmentation measurement. 'Images are available in colour online.'

fragmentation, the images are captured from the front, middle and back sections of each blast muck pile to ensure that the size distributions in the images represent the muck pile as a whole. Split Desktop (Split Engineering LLC 2016) is then deployed to digitalised the images and produce the CDF. The capture of images for blast fragmentation measurement is illustrated in Figure 2.

Methodology

Given an image of a blast muck pile, we first applied the Mask R-CNN model to find the rock fragments in it, locate their position and classify them. Finally, we compute the CDF to represent the measurement of fragmentation for that image. Our methodology rests on four key steps (Figure 3): (1) cropping the image into overlapping patches; (2) deploying trained Mask R-CNN model for rock fragment segmentation; (3) composing unique patches to the full detection image; (4) measure the fragmentation by computing CDF curve.

Dataset preparation

We started by collecting more than 200 images of blasting muck piles from the Nui Phao open-pit mine, as illustrated in Figure 2. The images vary with different sizes of [921 × 1312], [1080 × 1920], [2160 × 3840], [2408 × 4288], and [3056 × 5440] pixels. We manually annotated rock fragments on the images in detail using VGG Image Antonator (VIA) (Dutta et al. 2016) web tool to generate ground truth for training and evaluation steps. The ground truth is real rock fragments on the image, which are similar to the results of muck pile sieving. The annotations were stored in JSON files (www.JSON.org), mainly containing polygons' coordinates (yellow polygons in Figure 4 left) surrounding the rock fragment objects in the images. We cropped the image into overlapping patches with the size of [1024 × 1024] pixels and the overlap of [512 × 512] pixels to avoid running out of memory on the available graphics processing unit. From the original images, we generated 3894 patches containing about

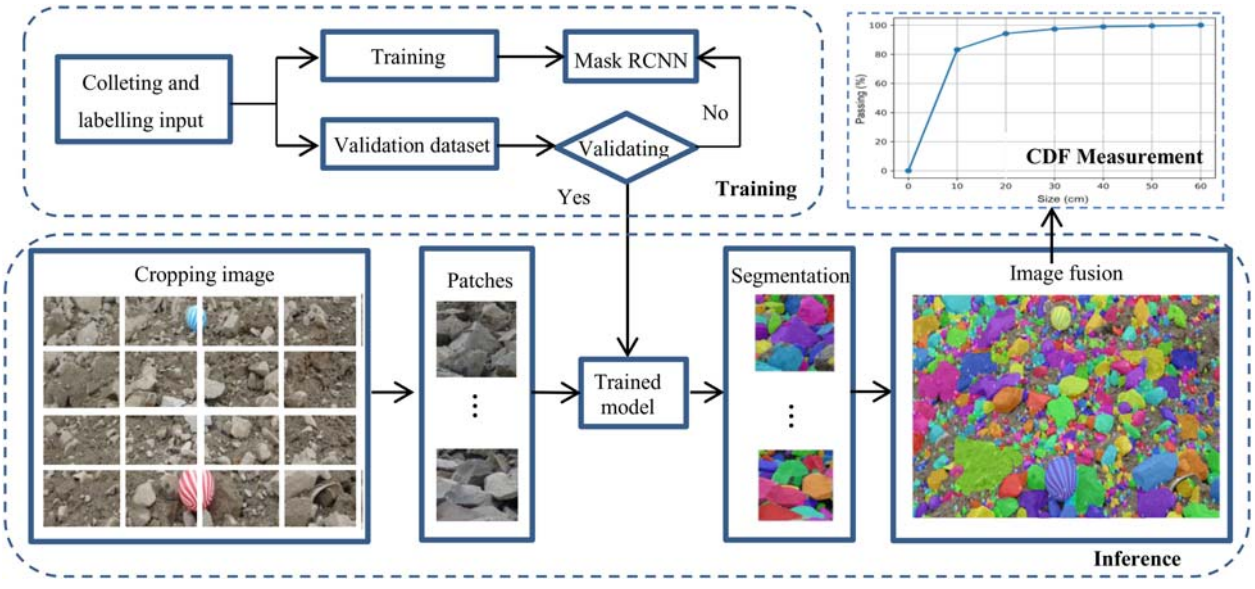

Figure 3. General workflow of automated measurement of blast fragmentation. 'Images are available in colour online.'

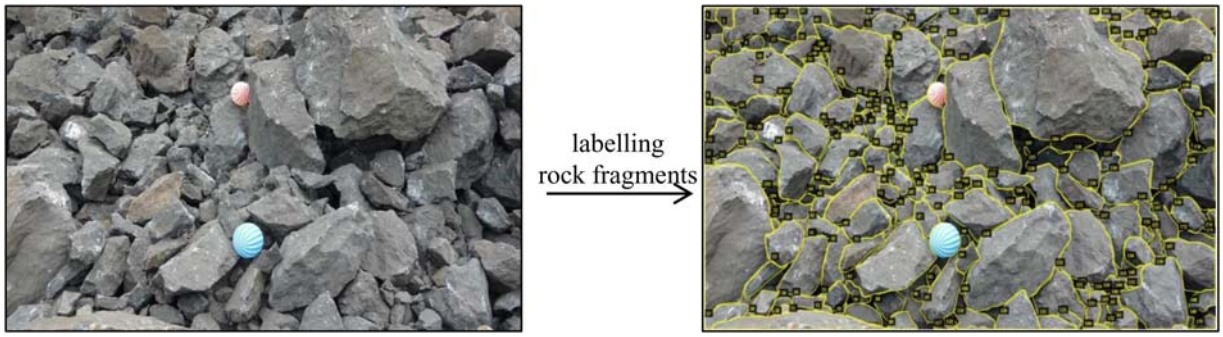

Figure 4. An example of a muck pile image (right) recorded at Nui Phao open-pit mine, Vietnam, containing two colour ball scaling objects and its rock fragments (left) labelled using VIA. 'Images are available in colour online.'

56,201 individual rock fragments. One fragment on a cropped patch was required.

For training the Mask RCNN model, we randomly partitioned the dataset, based on the ratio of 90:10, into the training dataset and validation dataset, respectively. Simultaneously, in the training process, we artificially enlarged the training dataset through standard augmentation techniques like mirroring, rotating, cropping, and up/downscaling to improve the ability of the model to generalise on what it has learned to new images.

Deep learning algorithm Mask R-CNN

In this study, we chose the Mask R-CNN algorithm (He et al. 2017) to detect and segment rock fragments within blast muck piles due to its simplicity and effectiveness. The Mask R-CNN is developed from Faster-RCNN (Ren et al. 2015).

It includes two stages as follows (He et al. 2017):

(1) scans the image to generate region proposals (the regions having the rock fragments);
(2) predicts three outputs (see Figure 5): class label (rock fragment or background); bounding-box (BB) (the locations of possible rock fragments in the image); and binary mask (*one* for rock fragments and *zero* for background) for each region of interest (RoI).

In terms of architecture (Figure 5), Mask R-CNN mainly deploys:

(1) Convolutional backbone architecture for feature extraction;
(2) Region Proposal Network (RPN) for generating RoI;
(3) RoI classifier for class prediction on each RoI;
(4) BB Regressor for refining RoI;
(5) Fully Convolutional Network (FCN) (Long et al. 2015) together with RoIAlign (Li et al. 2017) and bilinear interpolation for predicting pixel-accurate mask from each RoI.

In this study, we used a Feature Pyramid Network (FPN) (Lin et al. 2017) for the backbone architecture and Resnet 101 (He et al. 2016) for the head, as suggested by the authors. A detailed discussion of the Mask R-CNN algorithm can refer to He et al. (2017).

Training procedure

We extended the Matterport implementation of Mask R-CNN (Abdulla 2017), an open-source package built on Keras and Tensorflow. The training and inference procedure runs on the cloud service Google Colab (LLC Google) with Intel(R) Xeon(R) @ 2.20 GHz × one core with 64 Gb of main memory and a Tesla P100-PCIE-16GB graphics card with 12 Gb RAM. We configured the training with a mini-batch size of one image, 500 steps per epoch, a learning rate of 0.0001, a non-max suppression threshold of 0.2. Besides, a confidence threshold of 0.45 was set for evaluating how likely the found object was a rock fragment. For instance, at all proposal regions with a confident score of 0.45 or higher, a rock fragment is present. The readers can refer to the configuration file of Mask R-CNN on Github (https://github.com/matterport/Mask_RCNN) for the full descriptions of training parameter configuration.

Weights and bias are the learnable parameters inside the network. In the beginning, weights and bias are initialised randomly. Instead of training the Mask R-CNN from random initialisation, we used the Mask R-CNN's pre-trained weights for the COCO dataset (http://cocodataset.org/#home), which contains several thousand images. Our Mask R-CNN was trained with 100 epochs in which the first five epochs were used for training the network head (see Figure 5), and the remaining 95 epochs were used for training both the entire network. The classification loss (L_{cls}), BB loss (L_{box}), average binary cross-entropy loss (L_{mask}), regarding three outputs as illustrated in Figure 5, are used to describe the accuracy of these predictions during training. Thus, we

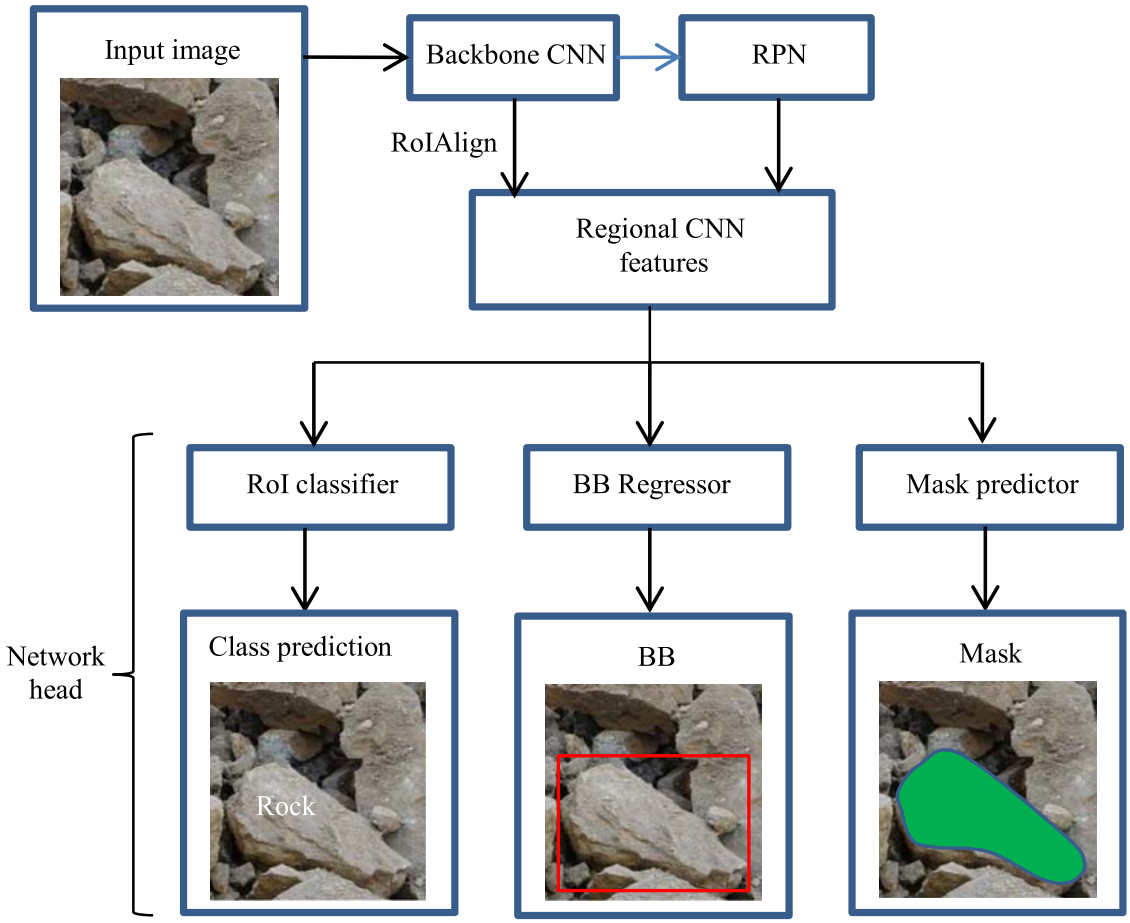

Figure 5. The implementation architecture of the Mask R-CNN. 'Images are available in colour online.'

attempt to minimise the overall loss

$$L = L_{cls} + L_{box} + L_{mask} \quad (1)$$

on each sampled RoI (He et al. 2017).

Image fusion

As shown in Figure 3, the trained Mask R-CNN model is trained to detect and segment rock fragments on overlapping patches. Hence, it is essential to fuse them into a global image to compute the final CDF. The problem is that some individual fragment segmentations are available on a patch that is also in other patches. To resolve this problem, we followed and modified the idea in Schenk et al. (2019). From the set of masks S generated by inferencing on overlapping patches, we searched the overlapping masks i with an area M_i in pixel and j with an area M_j in pixel, based on the overlapping BB. Then, we computed the general overlap area S_{ij} between each mask as:

$$S_{ij} = M_i \cap M_j \forall_{i,j} \in S \quad (2)$$

Subsequently, we computed the relative overlap ratios r_i and r_j for each mask using the equations:

$$r_i = S_{ij}/M_i;\ r_j = S_{ij}/M_j \quad (3)$$

If $r_i \geq \Delta$ and $r_j \geq \Delta$, we merge two masks into one since it likely the same fragment. We found that a large fragment, whose mask is larger than the size of a cropped patch, may be separated into some parts if we keep the mask with the highest confidence value (Schenk et al. 2019). For all other cases of r_i and r_j, there is probably no overlap or tiny overlap or a small fragment located beyond another. Hence, we include both masks i and j into S. Moreover, we implemented the experiments with various Δ values and found $\Delta = 0.5$ were the most suitable ones.

CDF computation

As described in section 'Introduction', the CDF is used to express the sieving process, where it computes the percentage of fragments passing through a known screening mesh size. Therefore, we are only interested in the smallest size of a fragment. Fragment size can be measured as an area of their polygon. However, areas are challenging to visualise, so fragment sizes commonly are represented as the smallest diameters of equivalent circles (D) or ellipse ($D_{\min}$), as shown in Figure 6.

If a fragment is equivalent to a circle with diameter D and area A, its smallest diameter can be calculated as:

$$\mathrm{D} = 2(\mathrm{A}/\pi)^{1/2} \quad (4)$$

Figure 6. Circle-equivalent diameter (left) and ellipse-equivalent diameter (right) of the fragment.

Table 1. Definition of True Positive (*TP*), False Positive (*FP*), and False Negative (*FN*). They were identified for varying threshold (*T*) of the confident score (*CS*) to measure whether the model detected a rock fragment. The *IoU* determine a rock fragment at the proposal region.

Model predictions compared to ground truth		Metrics
$CS \geq T$ (rock fragment detected)	$IOU > 0.5$ (rock fragment present)	*TP*
	$IOU \leq 0.5$ (no rock fragment present)	*FP*
$CS < T$ (no rock fragment detected), but rock fragment present		*FN*

Suppose a fragment is equivalent to an ellipse with two axes $D_{\max}$ and $D_{\min}$. In that case, we first use a marching squares method (Cubes 1987) to find the contour of the fragment and then implement the Fitzgibbon method (Fitzgibbon et al. 1999) to fit an ellipse around the fragment. The smallest diameter of the fragment is the minimum value of $D_{\max}$ and $D_{\min}$.

Accuracy evaluation

We implemented an assessment for the accuracy of the trained Mask R-CNN model and the computed CDF.

Evaluation of the trained Mask R-CNN

The averaged precision score (AP) and mean averaged precision score (mAP), as described below, are used to evaluate the model. These metrics are calculated by comparing the ground truth bounding box and segmentation mask with the model's predicted bounding box and segmentation mask. The higher the AP and mAP values, the more accurate the model is in its detection. Three steps are required to calculate these metrics, as follows:

(i) compute the Intersection over Union (IoU) to identify correct detections. Figure 7 explains the computation of IoU in which it is the proportion of the intersection and the BB output union by the model and the ground truth BB. Similarly, IoU values are calculated for the segmentation mask by using the intersection and union of the ground truth mask and the mask generated by the model. In this study, the determination of a rock fragment with an IoU value larger than 0.5 is considered correct detection, and vice versa.

(ii) calculate three object detection metrics: True Positive (*TP*), False Positive (*FP*), and False Negative (*FN*), as determined according to Table 1.

(iii) calculate two metrics: precision and recall, as shown in Equations (5) and (6). Precision is the percentage of correctly detected rock fragments of all rock fragments detected by the model. Recall is the ratio of correctly detected rock fragments of all ground truth rock fragments.

$$\text{Precision} = \frac{\text{TP}}{\text{TP} + \text{FN}} \tag{5}$$

$$\text{Recall} = \frac{\text{TP}}{\text{TP} + \text{FP}} \tag{6}$$

(iv) measure AP and mAP: At a fixed IoU = 0.5, the thresholds *T* of *CS* (Table 1) are varied to create the precision-recall curve *pr*. AP is defined as the mean precision over a set of eleven equally spaced recall values {0,0.1, … ,1} (Everingham et al. 2010):

$$AP = \frac{1}{11} \sum_{r \in \{0, 0.1, \ldots, 1\}} pr_{interp}(r) \tag{7}$$

with pr_{interp} is interpolated from the precision-recall curve *pr* by taking the maximum precision values for which the corresponding recall exceeds *r*:

$$pr_{interp}(r) = \max_{r' \geq r} \{p(r')\}, r\hat{I}\{0, 0.1, \ldots, 1\} \tag{8}$$

where *p(r')* is the measured precision at recall *r'*.

Finally, an average of AP values at ten different IoUs {0.5, 0.55, … ,0.95,1} is done to provide a single value of mAP.

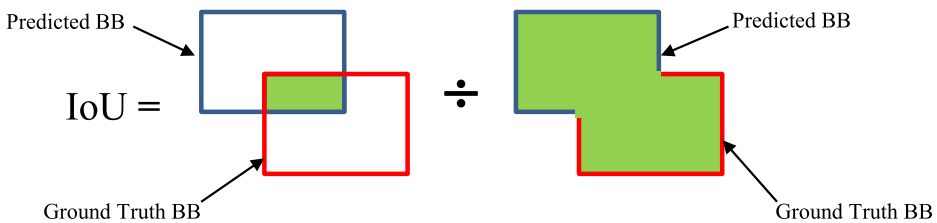

Figure 7. IoU calculation for BBs. 'Images are available in colour online.'

Evaluation of CDF measurement

We compared our measurement method to the commercial SplitDesktop software to evaluate fragmentation results. SplitDesktop was set to automatically delineates rock fragments using its image filter. Since the SplitDesktop approximates the rock fragments as elliptical objects (La Rosa et al. 2001), we also applied this strategy to compute the CDF sieving curve, as discussed in section 'CDF computation'.

Results

Training optimisation

We recorded different loss components during the training and evaluation process. The optimum Mask R-CNN model was chosen using an early stopping strategy in which the training process is terminated at the point when the overall loss starts to degrade. As shown in Figure 8(a), the lowest overall loss value measured on the evaluation dataset was gained after 80 epochs before rebounding. Whereas the overall training loss values continued to decrease, indicating that after 80 epochs, the model tended to fit the training data rather than learn to generalise rock fragments' features. The Mask R-CNN class loss values on the validation dataset in Figure 8(b) eventually stopped learning in the early stages. Although the bounding box loss and mask binary cross-entropy loss in Figure 8(c,d) still fluctuated around their training loss to the final epochs, they did not contribute too much to the overall validation loss.

Table 2. Evaluation metrics: averaged precision score (AP) and mean averaged precision (mAP) of the trained model and the Mask R-CNN model (He et al. 2017) using Resnet101-FPN backbone trained on the COCO dataset for bounding boxes and segmentation masks.

Metric	Mask RCNN trained on fragmentation dataset		Mask RCNN trained on COCO dataset	
	Bounding box	Mask segmentation	Bounding box	Mask segmentation
AP	0.921	0.852	0.603	0.573
mAP	0.550	0.428	0.382	0.354

Detection and segmentation of rock fragments

Table 2 reports the evaluation metrics AP and mAP for the trained model on the full dataset. Compared with the model trained on the COCO dataset (He et al. 2017), the trained model performed well to detect bounding boxes and segmentation mask with the AP scores are 0.921 and 0.852, respectively. Whereas the more strict performance measure mAP could be considered moderate to high. The mAP scores of 0.550 for bounding box and 0.428 for mask segmentation indicate that the rock fragments were detected, but their outlines did not fit well due to the fuzzy shape of the rock fragments.

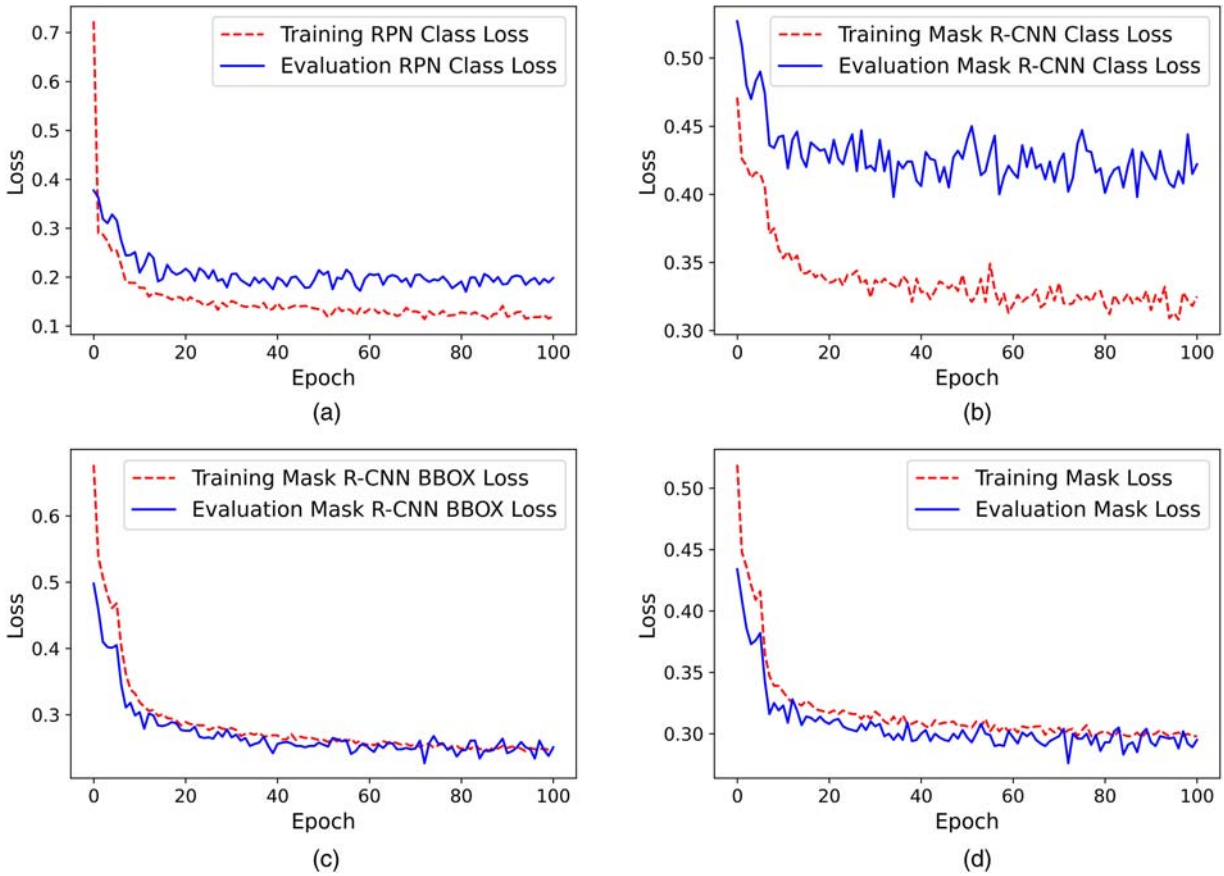

Figure 8. Loss graphs for Mask R-CNN training and evaluation. 'Images are available in colour online.'

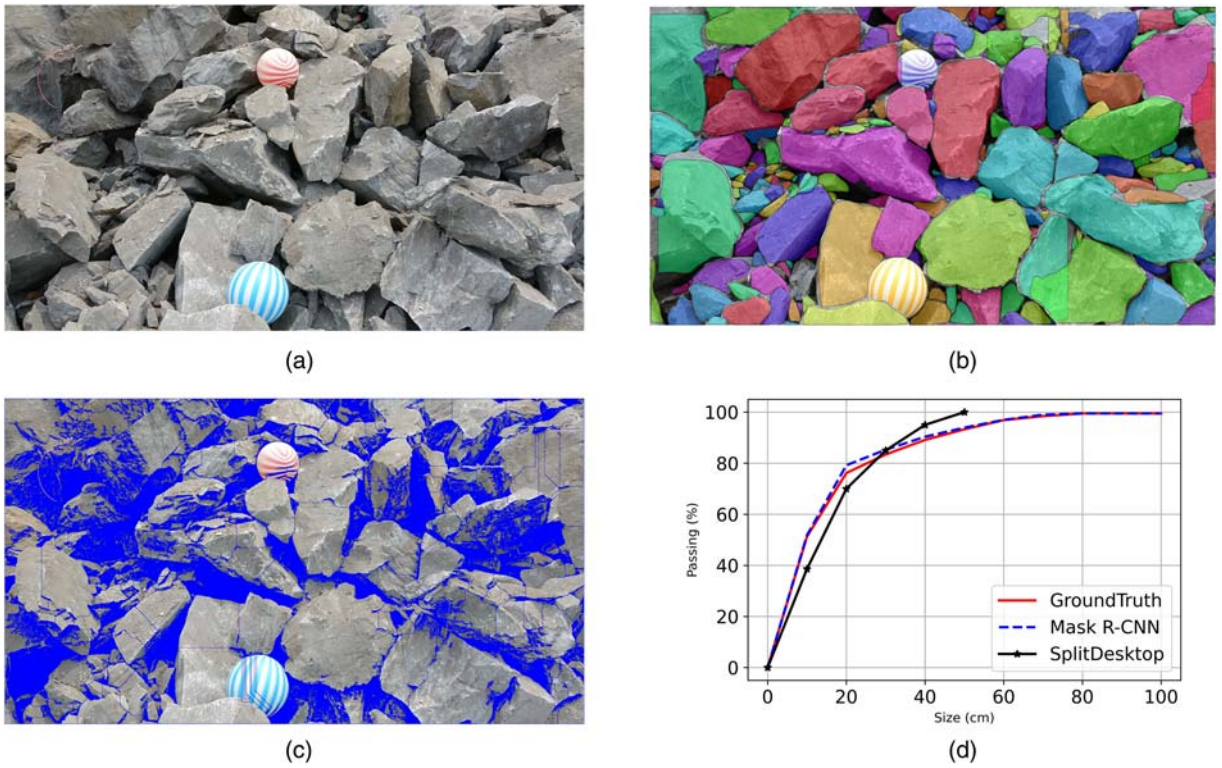

Figure 9. Prediction results of boulder rock fragments using Mask R-CNN model and SplitDesktop. 'Images are available in colour online.'

Fragmentation measurement

We conducted case studies from the validation dataset with different fragment sizes and compositions to evaluate the accuracy of the measurement method. In total, we tested four typical image scenes: (1) boulder rock image; (2) densely packed rock image; (3) coloured rock texture image; (4) dust mixing with rocks image. We compared our measurement method to the commercial SplitDesktop software to evaluate fragmentation results.

(1) Boulder rock image

This case study illustrates a fragmentation measurement result on the boulder rock image (Figure 9(a)). Figure 9(d) shows our fragmentation measurement using the Mask R-CNN model was close to the CDF computed on ground truth. As shown in Figure 9(c, d), the CDF caused by SplitDesktop was steeper in the upper part where the large fragments tend to be separated into smaller pieces, while it was more gentle in the lower part where the small fragments were merged into larger ones. The trained Mask R-CNN model (Figure 9(b)) successfully detected small fragments (smaller than 20 cm). The error occurred for the larger fragments, likely due to the image fusion process used to join the image cropping patches.

(2) Densely packed rock image

In case study 2, the number of fragments on the image increased significantly (Figure 10(a)). Figure 10(d) shows that the CDF computed by our measurement was slightly different from the ground truth. Similar to case study 1, SplitDesktop regularly merged smaller fragments into larger ones, making its CDF utterly different from the ground truth, as shown in Figures 10(c,d). Therefore, it requires a tedious effort to edit the delineation manually.

(3) Coloured rock texture image

In case study 3, we continue to test our measurement on a rock image containing rock fragments with various colour texture (Figure 11(a)). Consequently, the effect of rock texture did not dramatically affect the trained Mask R-CNN's performance (Figure 11(b)). In contrast, SplitDesktop merged adjacent fragments with the same colour into larger ones (Figure 11(c)) and generated a more gentle CDF curve than the ground truth (Figure 11(d)).

(4) Dust mixing with rocks image

In Figure 12(a), the whole rock image is not fully occupied by the fragments. Parts of non-fragments regions are background or covered by dust. Based on the ground truth image observation, the trained Mask R-CNN was challenging to detect the fragments covered by the dust, even though they can be distinguished by human vision. In Figure 12(b,c), the trained Mask R-CNN could determine fore and

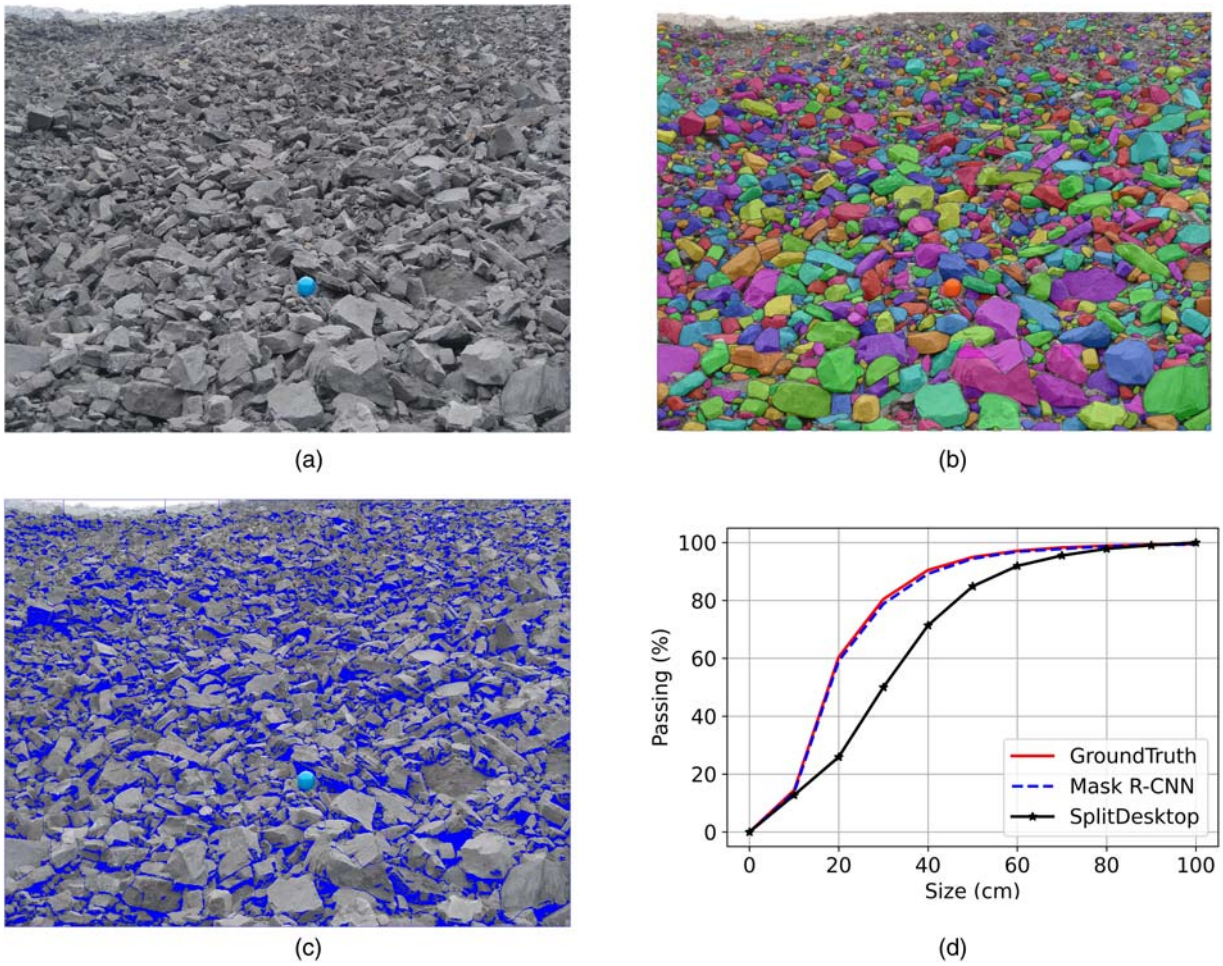

Figure 10. Prediction results of densely packed rock fragments using Mask R-CNN model and SplitDesktop. 'Images are available in colour online.'

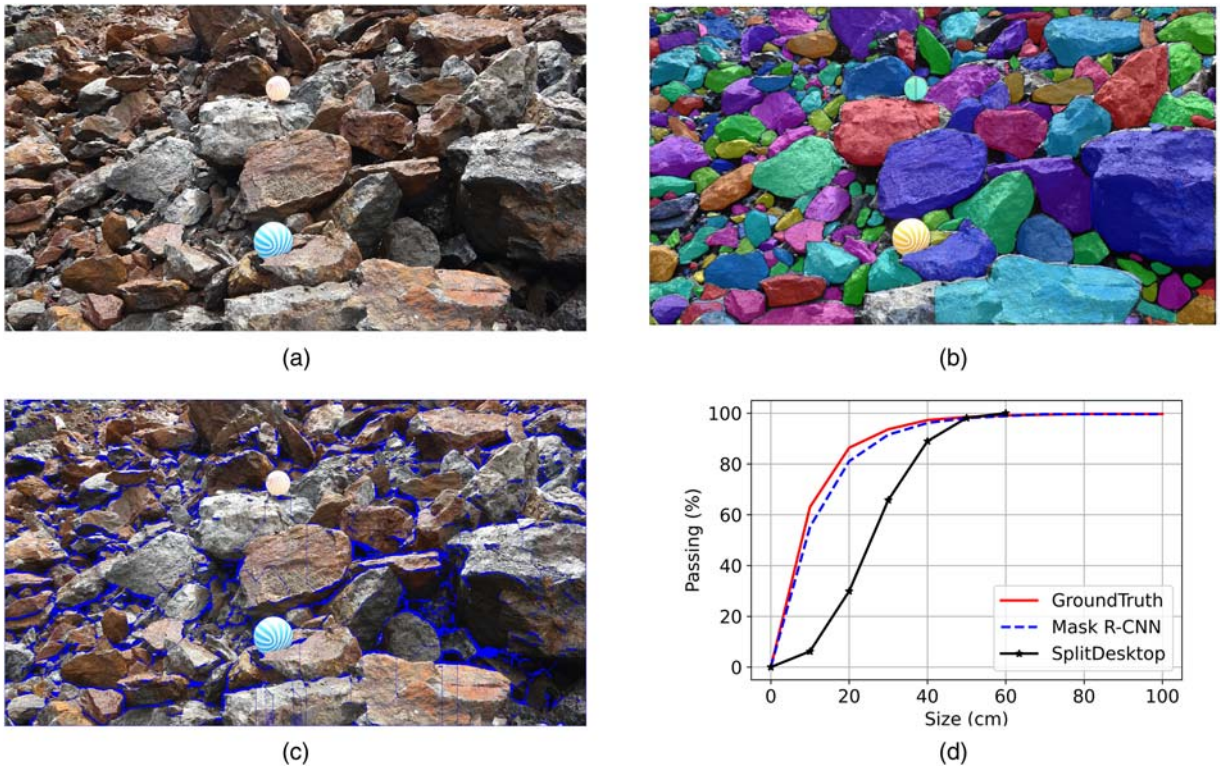

Figure 11. Prediction results of coloured rock texture image using Mask R-CNN model and SplitDesktop. 'Images are available in colour online.'

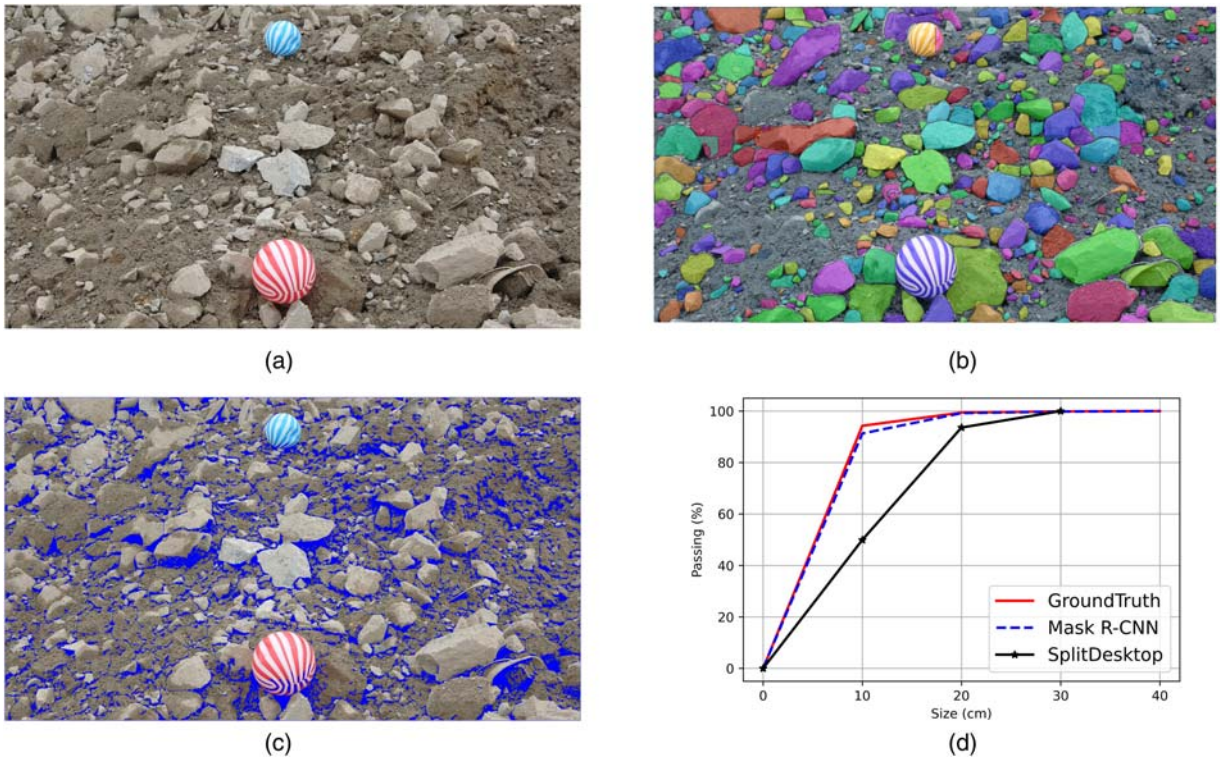

Figure 12. Prediction results of dust mixing with rock fragments using Mask R-CNN model and SplitDesktop. 'Images are available in colour online.'

background while SplitDesktop over-segmented the fragments and interpreted the background as large fragments. Consequently, the CDF computed by our measurement was close to the ground truth, while SplitDesktop produced an incorrect and uniform distribution (Figure 12(d)).

Discussion

Blasting fragmentation analysis is a difficult task and relies heavily on the quality of the segmentation results. Since rock fragment images vary from one to another, developing a segmentation algorithm for all kinds of rock fragment images without using a manual edition is challenging. This study selected Mask R-CNN, a deep learning model, to conduct an automated instance segmentation of the blasting fragments. The training and validation dataset was collected from the real mine blasts and cropped into smaller ones to reduce memory utilisation. A fusion approach was developed to combine the inference images into the final segmentation. The rock fragments in the images were successfully detected and segmented with high AP values for bounding box (0.921) and mask segmentation (0.852). Whereas the more strict performance measure mAP could be considered moderate to high. However, future efforts should compare Mask R-CNN's performance to other similar segmentation methods such as U-Net (Ronneberger et al. 2015) or MaskLab (Chen et al. 2018) in fragmentation measurement. In this study, we applied default hyperparameters and early stopping to minimise overfitting in the training process. Hence, it would also be valuable to conduct comprehensive experiments on model optimisation to improve training time and accuracy.

Image processing methods based on edge segmentation algorithms have been the most widely used in blast fragmentation measurement. In many instances, these methods are sensitive to image features such as fragment distribution (Figure 9 and 10), texture on fragments (Figure 11), or image background (Figure 12). The trained Mask R-CNN model successfully utilised the multi-level feature representations learned from the training data to overcome these disadvantages. With their AP and mAP scores, the case studies clarify the model's robustness to rock fragment detection. However, there can be a reduction of mask segmentation when the image's complexity increases. There are likely two main reasons for this problem: (1) lack of training data; (2) fragments have fuzzy boundaries or blend with the background; and (3) the spatial resolution of the image is not suitable for inference. We proposed two possible solutions to improve the mask segmentation ability: (1) enriching training dataset from different sources; (2) enhancing the spatial resolution of the image to be suitable for inference. For instance, the image in Figure 13(a) has a resolution of 1204×2144, and the prediction result is illustrated in Figure 13(b). We doubled its resolution to 2048×4288, and the inference result is shown in

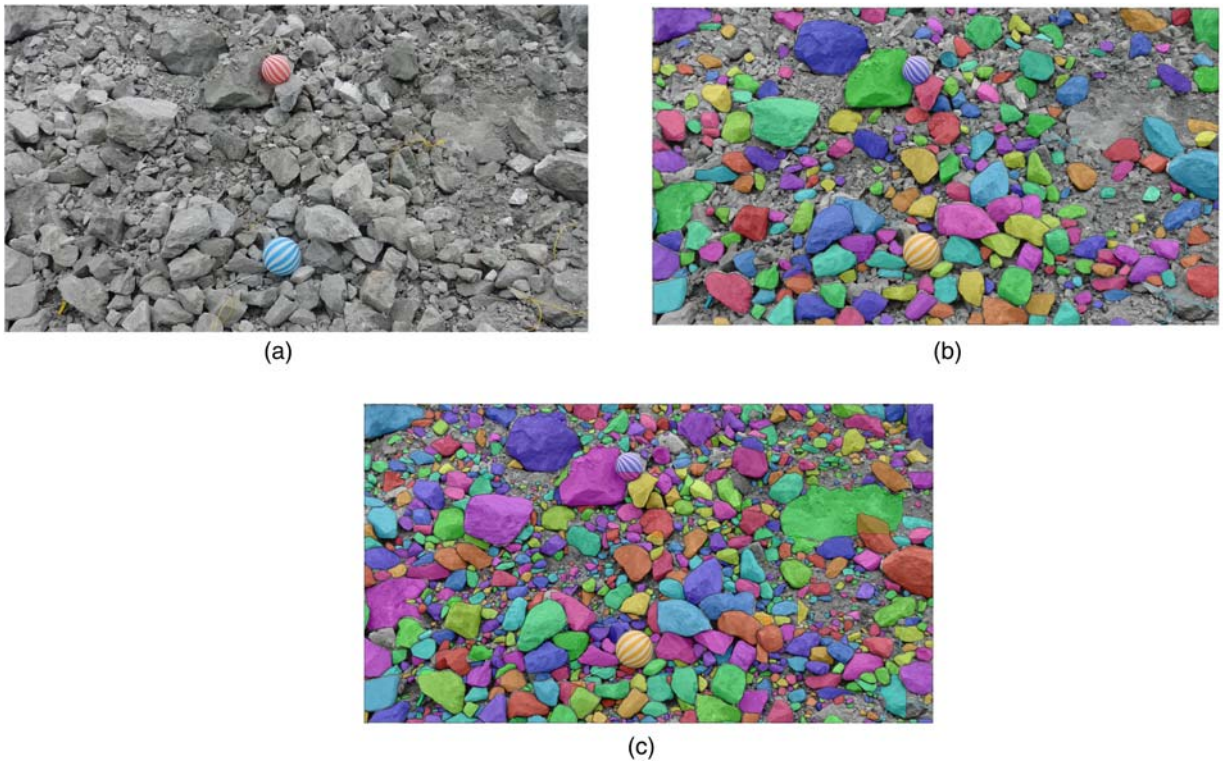

Figure 13. Fragment segmentation improvement when resizing the original image. 'Images are available in colour online.'

Figure 13(c). It is clearly visible that the number of detected fragments significantly increases, enabling the CDF computation accuracy.

Conclusions

There are significant economic incentives to measure blast fragmentation in mining. However, the measurement is still time-consuming and heavily relies on user interaction and experience. This study provided an automatic measurement method for blast fragmentation in Nui Phao open-pit mine. The method utilises the deep learning model Mask R-CNN, which was trained and validated using the muck pile images captured in the mine. It is demonstrated that the proposed method can detect and segment rock fragments with a high average precision score for bounding box (0.921) and mask segmentation (0.852) for a given IoU threshold of 0.5.

Our future work will enrich the dataset and model optimisation by testing various combinations of training hyperparameters. Since we have training weights for rock blasting images captured using regular cameras, we also want to challenge our model with the UAV images or ones captured on other mining equipment such as excavators, trucks, or crushers.

Acknowledgements

We also thank Nui Phao mining company, Vietnam, for providing the image dataset and the team of Mask-RCNN for sharing codes on Github.

Disclosure statement

No potential conflict of interest was reported by the author(s).

Funding

This work has been supported by Quang Ninh University of Industry and Hanoi University of Mining and Geology, Vietnam.

ORCID

Trong Vu http://orcid.org/0000-0001-8765-387X

References

Abdulla W. 2017. Mask R-CNN for object detection and instance segmentation on Keras and TensorFlow. https://github.com/matterport/Mask_RCNN.2017.

Chakraborty AK, Raina AK, Ramulu M, Choudhury PB, Haldar A, Sahu P, Bandopadhyay C. 2004. Parametric study to develop guidelines for blast fragmentation improvement in jointed and massive formations. Eng Geol. 73(1–2):105–116.

Chen LC, Hermans A, Papandreou G, Schroff F, Wang P, Adam H. 2018. Masklab: Instance segmentation by refining object detection with semantic and direction features. In Proceedings of the IEEE Conference on Computer Vision and Pattern Recognition. Salt Lake City, UT, USA; p. 4013–4022.

Cubes M. 1987. A high resolution 3D surface construction algorithm. In Proceedings of the 14th Annual Conference on Computer Graphics and Interactive

Techniques; July. New York (NY): Association for Computing Machinery. p. 163–169.
Dai J, He K, Li Y, Ren S, Sun J. 2016. Instance-sensitive fully convolutional networks. In European Conference on Computer Vision; Oct 8. Cham: Springer. p. 534–549.
Dutta A, Gupta A, Zissermann A. 2016. VGG Image Antonator (VIA). [accessed 2020 June 2]. http://www.robots.ox.ac.uk/~vgg/software/%0Avia/via.html.
Enayatollahi I, Bazzazi AA, Asadi A. 2014. Comparison between neural networks and multiple regression analysis to predict rock fragmentation in open-pit mines. Rock Mech Rock Eng. 47(2):799–807.
Everingham M, Van Gool L, Williams CK, Winn J, Zisserman A. 2010. The pascal visual object classes (voc) challenge. Int J Comput Vision. 88(2):303–338.
Fitzgibbon A, Pilu M, Fisher RB. 1999. Direct least square fitting of ellipses. IEEE Trans Pattern Anal Mach Intell. 21(5):476–480.
Girshick R. 2015. Fast r-cnn. Proceedings of the IEEE International Conference on Computer Vision. Santiago, Chile; p. 1440–1448.
He K, Gkioxari G, Dollár P, Girshick R. 2017. Mask r-cnn. Proceedings of the IEEE International Conference on Computer Vision. Venice, Italy; p. 2961–2969.
He K, Zhang X, Ren S, Sun J. 2016. Proceedings of the 2016 IEEE Conference on Computer Vision and Pattern Recognition. Las Vegas, NV, USA: IEEE: Piscataway, NJ, USA, 2016; p. 770–778. doi:10.1109/CVPR.2016.90.
Hunter GC, McDermott C, Miles NJ, Singh A, Scoble MJ. 1990. A review of image analysis techniques for measuring blast fragmentation. Min Sci Technol. 11 (1):19–36.
Kulatilake PH, Qiong W, Hudaverdi T, Kuzu C. 2010. Mean particle size prediction in rock blast fragmentation using neural networks. Eng Geol. 114(3–4):298–311.
La Rosa DM, Girdner K, Valery W, Abramson S. 2001. Recent applications of the SPLIT on-line image analysis system. p. 15–19.
Li Y, Qi H, Dai J, Ji X, Wei Y. 2017. Fully convolutional instance-aware semantic segmentation. Proceedings of the IEEE Conference on Computer Vision and Pattern Recognition. Honolulu, HI, USA; p. 2359–2367.
Lin TY, Dollár P, Girshick R, He K, Hariharan B, Belongie S. 2017. Feature pyramid networks for object detection. Proceedings of the IEEE Conference on Computer Vision and Pattern Recognition. Honolulu, HI, USA; p. 2117–2125.
LLC Google. Google Colab. [accessed 2020 June 2]. https://colab.research.google.com/notebooks/intro.ipynb.
Long J, Shelhamer E, Darrell T. 2015. Fully convolutional networks for semantic segmentation. Proceedings of the IEEE Conference on Computer Vision and Pattern Recognition. Boston, MA, USA; p. 3431–3440.
Monjezi M, Rezaei M, Varjani AY. 2009. Prediction of rock fragmentation due to blasting in Gol-E-gohar iron mine using fuzzy logic. Int J Rock Mech Min Sci. 46 (8):1273–1280.
Onederra I, Mardones F, Scherpenisse C. 2010. Application of stochastic approach to blast fragmentation modelling. Min Technol. 119(4):221–232.
Onederra I, Thurley MJ, Catalan A. 2015. Measuring blast fragmentation at esperanza mine using high-resolution 3D laser scanning. Min Technol. 124(1):34–36.
Ouchterlony F, Sanchidrián JA. 2019. A review of development of better prediction equations for blast fragmentation. J Rock Mech Geotech Eng. 11(5):1094–1109.
Pinheiro PO, Collobert R, Dollár P. 2015. Learning to segment object candidates. arXiv preprint arXiv:1506.06204.
Pinheiro PO, Lin TY, Collobert R, Dollár P. 2016. Learning to refine object segments. European Conference on Computer Vision; Oct 8. Cham: Springer. p. 75–91
Ren S, He K, Girshick R, Sun J. 2015. Faster r-cnn: towards real-time object detection with region proposal networks. arXiv preprint arXiv:1506.01497.
Ronneberger O, Fischer P, Brox T. 2015. U-net: convolutional networks for biomedical image segmentation. International Conference on Medical Image Computing and Computer-Assisted Intervention; Oct 5. Cham: Springer. p. 234–241.
Sayadi A, Monjezi M, Talebi N, Khandelwal M. 2013. A comparative study on the application of various artificial neural networks to simultaneous prediction of rock fragmentation and backbreak. J Rock Mech Geotech Eng. 5 (4):318–324.
Schenk F, Tscharf A, Mayer G, Fraundorfer F. 2019. Automatic muck pile characterization from UAV images. ISPRS annals of the photogrammetry. Remote Sens Spat Inf Sci. 4(W5):163–170.
Shi XZ, Jian ZH, Wu BB, Huang D, Wei WE. 2012. Support vector machines approach to mean particle size of rock fragmentation due to bench blasting prediction. Trans Nonferrous Met Soc China. 22(2):432–441.
Siddiqui FI. 2009. Measurement of size distribution of blasted rock using digital image processing. Eng Sci. 20 (2):81–93.
Split Engineering LLC. 2016. Split-desktop 3.0 manual.
Sudhakar J, Adhikari GR, Gupta RN. 2006. Comparison of fragmentation measurements by photographic and image analysis techniques. Rock Mech Rock Eng. 39 (2):159–168.
Thornton DM, Kanchibotla SS, Esterle JS. 2001. A fragmentation model to estimate ROM size distribution of soft rock types. Proceedings of the Twenty-Seventh Annual Conference on Explosives and Blasting Technique, Vol I; Jan 1. International Society of Explosives Engineers. p. 41–53.